Landslide precipitation thresholds in Rwanda

Uwihirwe, Judith; Hrachowitz, Markus; Bogaard, Thom A.

Important note
To cite this publication, please use the final published version (if applicable).
Please check the document version above.

Judith Uwihirwe · Markus Hrachowitz · Thom A. Bogaard

Landslide precipitation thresholds in Rwanda

Abstract Regional empirical-statistical thresholds indicating the precipitation conditions initiating landslides are of crucial importance for landslide early warning system development. The objectives of this research were to use landslide and precipitation data in an empirical-statistical approach to (1) identify precipitation-related variables with the highest explanatory power for landslide occurrence and (2) define both trigger and trigger-cause based thresholds for landslides in Rwanda, Central-East Africa. Receiver operating characteristics (ROC) and area under the curve (AUC) metrics were used to test the suitability of a suite of precipitation-related explanatory variables. A Bayesian probabilistic approach, maximum true skill statistics and the minimum radial distance were used to determine the most informative threshold levels above which landslide are high likely to occur. The results indicated that the event precipitation volumes E, cumulative 1-day rainfall (RD_1) that coincide with the day of landslide occurrence and 10-day antecedent precipitation are variables with the highest discriminatory power to distinguish landslide from no landslide conditions. The highest landslide prediction capability in terms of true positive alarms was obtained from single rainfall variables based on trigger-based thresholds. However, that predictive capability was constrained by the high rate of false positive alarms and thus the elevated probability to neglect the contribution of additional causal factors that lead to the occurrence of landslides and which can partly be accounted for by the antecedent precipitation indices. Further combination of different variables into trigger-cause pairs and the use of suitable thresholds in bilinear format improved the prediction capacity of the real trigger-based thresholds.

Keywords Landslide · Precipitation thresholds · Trigger-based thresholds · Trigger-cause-based thresholds

Introduction

Landslides are one of the world's most widely occurring natural hazards, causing high number of human casualties and considerable economic damage (Nadim et al., 2006; Petley 2012; Froude and Petley 2018). Global landslide fatalities have been increasing following the increase in population density (Petley 2012), changes in seasonal rainstorm pattern and human activities (Froude and Petley 2018). Rainfall is likely to be one of the major triggers of landslide-induced fatalities in mountainous areas as it is the case in many tropical African countries including Rwanda (Monsieurs et al. 2018b, c). However, a bias in geographical distribution of studies on landslides induced by climate factors including but not limited to changes in seasonal rainfall was found with a major gap in Africa (Gariano and Guzzetti 2016). To reduce rainfall-induced landslide casualties, empirical and physically based dynamic models to forecast landslide hazards have been proposed and adopted to define rainfall induced-landslide early warning thresholds. These thresholds indicate the minimum rainfall, groundwater levels, soil moisture contents and other hydrological conditions

potentially linked to landslide initiation at local, regional and global scales. The physical, process-based models aim to understand and describe the dynamic processes responsible for landslide initiation. They typically combine slope stability and hydrological models in which dynamic hydrological processes are used to evaluate slope failure probabilities (Anderson and Lloyd 1991; Montgomery and Dietrich 1994; van Beek 2002; Rosso et al. 2006; Kuriakose et al. 2009). However, physically based dynamic models require high-resolution spatio-temporal data, which are largely unavailable in most of the areas worldwide. Applications of this type of models are thus highly limited to few regions with sufficient data and typically to local scales only (Aleotti 2004).

Due to their less detailed data requirements, empirical-statistical models have been widely adopted to define the precipitation induced-landslide early warning thresholds at local (Crozier 1999; Prenner et al. 2018), national (Robbins 2016; Peruccacci et al. 2017), regional (Monsieurs et al. 2018a) and global scales (Caine 1980; Guzzetti et al. 2008). The empirical-statistical models typically relate precipitation characteristics, such as antecedent precipitation, cumulative event precipitation, precipitation intensity and precipitation duration or combination thereof to the occurrence of landslides. Despite the considerably lower data requirements of empirical-statistical threshold models, landslide initiation thresholds still remain poorly explored and defined throughout Africa (Gariano and Guzzetti 2016). This is due to the lack of accurate and complete landslide inventories and insufficient spatio-temporal resolution of the available precipitation data (Monsieurs et al. 2018c, b). The recent efforts by LIWEAR (Landslide Inventory for the central section of the Western branch of the East African Rift) as part of NASA's GLC (Global Landslide Catalogue) to systematically document landslides may partially solve the landslide data scarcity in Africa (Monsieurs et al. 2018c). Despite that, however, many landslide events are likely to be missed in the inventory due to the fact that for Africa mostly only newspapers, government reports and other media are used as a source for landslide inventory. While the reliance on these data sources is likely to result in a bias towards large and/or impactful landslides that may involve casualties and economic damage, this landslide inventory can nevertheless serve as basic starting point to define rainfall thresholds for landslide initiation in African countries.

Despite the limited research devoted to landslides in Africa, a number of landslide initiation rainfall thresholds have been proposed in the past (Piller 2016; Monsieurs et al. 2018a, 2019). Those thresholds are mainly inferred from empirical methods which are based on statistical analysis of historical rainfall characteristics and landslides inventories to distinguish the landslide conditions from no-landslide conditions. However, many limitations, constraints and uncertainties associated with empirical thresholds have been highlighted (Peres et al. 2017; Prenner et al. 2018; Bogaard and Greco 2018). Some limitations are due to the fact

that empirical thresholds are mainly based on the rainfall event during which a landslide occurred, which is in reality the actual landslide trigger. Hereafter, these thresholds are therefore referred to as *landslide trigger-based thresholds* with various timescales depending on rainfall intensity, volume or event duration. Such landslide trigger-based thresholds include the intensity-duration (*I-D*) (Caine 1980; Guzzetti et al. 2007, 2008; Ma et al. 2015; Hong et al. 2017; Roccati et al. 2018), event-duration (*E-D*) and event-intensity (*E-I*) (Peruccacci et al. 2017; Robbins 2016). The landslide trigger-based thresholds have been increasingly recognised to neglect the causal hydrological processes that predispose the slope to failure (Peres et al. 2017; Bogaard and Greco 2018; Mostbauer et al. 2018). To include this, a number of researchers considered the possible hydrological causes in terms of antecedent precipitation, catchment storage, soil moisture indices and or soil water status prior to the landslide triggering event or storm (Crozier 1999; Glade 2000; Aleotti 2004; Ciavolella et al. 2016; Mostbauer et al. 2018). These temporally variable hydrological conditions define the hydrological predisposition of a region to landslide occurrence and are thus, besides its geomorphological predisposition the root cause of landslide occurrence in a region. These hydrological conditions are defined prior to the landslide triggering conditions and then combined to make *landslide trigger-cause-based thresholds*.

The concept of the landslide trigger-cause framework was recently proposed by Bogaard and Greco (2018) and has been adopted using either in situ observed or modelled soil moisture to define the landslide hydro-meteorological thresholds (e.g. Mirus et al. 2018a, b; Prenner et al. 2018). Similar concepts were also adopted in other studies (e.g. Crozier 1999; Glade 2000; Aleotti 2004; Ciavolella et al. 2016; Mostbauer et al. 2018; Prenner et al. 2019). Mirus et al. (2018b) used the prior in situ soil saturation as a cause and the recent cumulated rainfall as trigger to define bilinear thresholds for landslide warning in Portland. The concept of bilinear thresholds was proposed by Mirus et al. (2018a) based on its predictive capacity as compared with the more commonly used univariate linear thresholds. One of the constraints of the hydro-meteorological/cause-trigger concept is indeed that one has to explore a wide range of combinations of explanatory variables which may be different based on landslide pre-disposing and triggering factors. The objective of this research is to use landslide and precipitation data in an empirical-statistical approach to define cause-trigger-based thresholds for landslides in Rwanda. Specifically, in this paper we aim to:

i. identify precipitation-related variables with the highest explanatory power for landslide occurrence in Rwanda
ii. quantify both, landslide trigger-based and cause-trigger-based thresholds as first step towards robust landslide early warning systems in Rwanda>

Study area description

Rwanda is a landlocked country geographically located between 1–3° S and 28–31° E in Central-Eastern Africa, characterised by tropical climate and pronounced relief. It is bounded by Uganda on the North, Burundi in the South, Tanzania on the East and Democratic Republic of Congo on the West (Fig. 1). It is topographically dominated by the volcanic highlands located over the North and Western regions and lowlands in the Savannah region located in east and southeast of the country as shown in Fig. 2. The highland region receives abundant rainfall with a long-term mean > 1200 mm year^{-1} while this reduces to < 1000 mm year^{-1} in the savannah region (Fig. 1). The country has two rainy seasons, the longer one extending from March through mid-May and the shorter one from mid-September to mid-December. Among the factors known to influence rainfall in Rwanda are subtropical anticyclones, tropical cyclones, monsoons, El Niño Southern Oscillation (ENSO), large water bodies and topography (Ngarukiyimana et al. 2017). Those factors expose Rwanda to variable weather, associated with frequent extreme rainfall events and the prolonged wet season that lead to flooding and landslide hazards.

The geology of Rwanda consists of Precambrian metasedimentary rocks mainly quartzite, sandstones and shales intruded by granites. Granitic-gneisses and migmatites are dominants in eastern Rwanda while Neogene and Quaternary volcanic deposits are dominants in northwest and southwest. The western Rift consists of alluvium and lake sediments of Quaternary age. The main lithological units in landslide area include mica schists and pegmatite rocks (Fig. 3) which are unstable due to rapid weathering, easy splitting along the joints and bedding planes and loss of strength induced by the high content of mica. Despite limited research on the impact of tectonic and seismic movement on landslides in Rwanda, the country is located in a tectonic region whose epicentre is located in Kivu Lake bordering the western part of Rwanda and Democratic Republic of Congo. The northwest part of the country is occupied by a volcanic chain which is seismically active. This makes Rwanda, especially the western and northwest regions, susceptible to earthquakes mentioned as one of the landslide causes in the East African Rift by Monsieurs et al. (2018c).

In part of Mukungwa catchment (756 km²) located in northwestern part of Rwanda, active and inactive landslides were recorded. The recorded landslides were classified as rotational slide (34%), flow (26%), translational slide (17%), fall (15%) and complex type of mass movement (7%) and involving mainly debris and earth materials. The typical landslide areal extent varied from 2.8×10^1 to 4.4×10^5 m² with an intensity of failure volume estimated between 1.3×10^1 and 5.8×10^6 m³ associated with a total landslide mobilization rate of about 21 mm year^{-1}. The main type of soils involved in mass movement is largely Umbric and Haplic acrisols (Dewitte et al. 2013) characterised by high clay content in deep layers acting as an impermeable layer and thus, creating perched ground water and high pore water pressure in the overlaying soil layers. Rwanda has undergone significant land use changes over the last decades (Nambajimana et al. 2020) which may have also induced change in landslide intensity. The Landsat-8 and sentinel images (1990–2016), accessed from the regional centre for mapping resources and development (http://opendata.rcmrd.org/search?q=RWANDA%20LANDSAT%20), indicated a forest land decrease from about 43 to 14% while agricultural land raised from about 25 to 53%.

Landslide data

The available data includes the Rwanda landslide inventory partially provided by the LIWEAR project and rainfall time series provided by Rwanda meteorological agency.
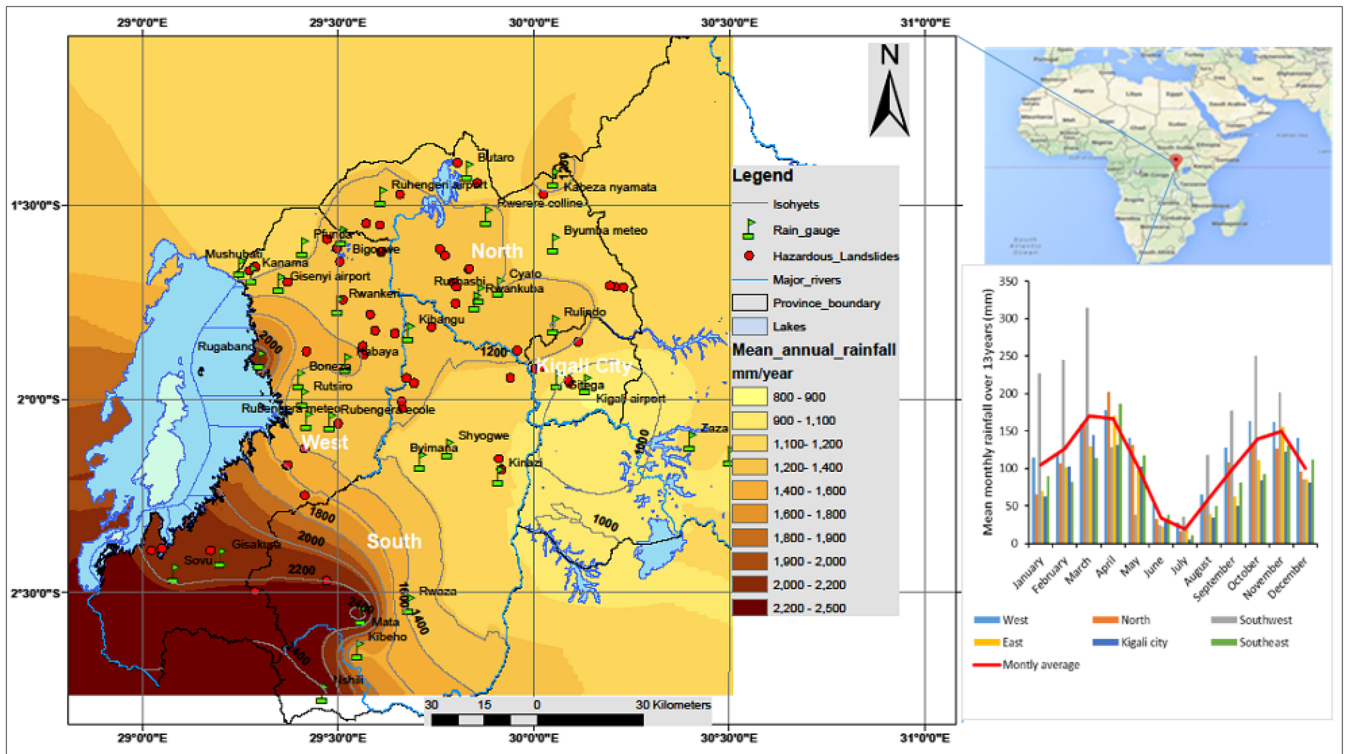
Fig. 1 Location of the study area, with spatial distribution of mean annual rainfall and recorded landslides from 2006 to 2018 (red dots). In the side panel, mean monthly rainfall per regions is shown for the 2006–2018 period
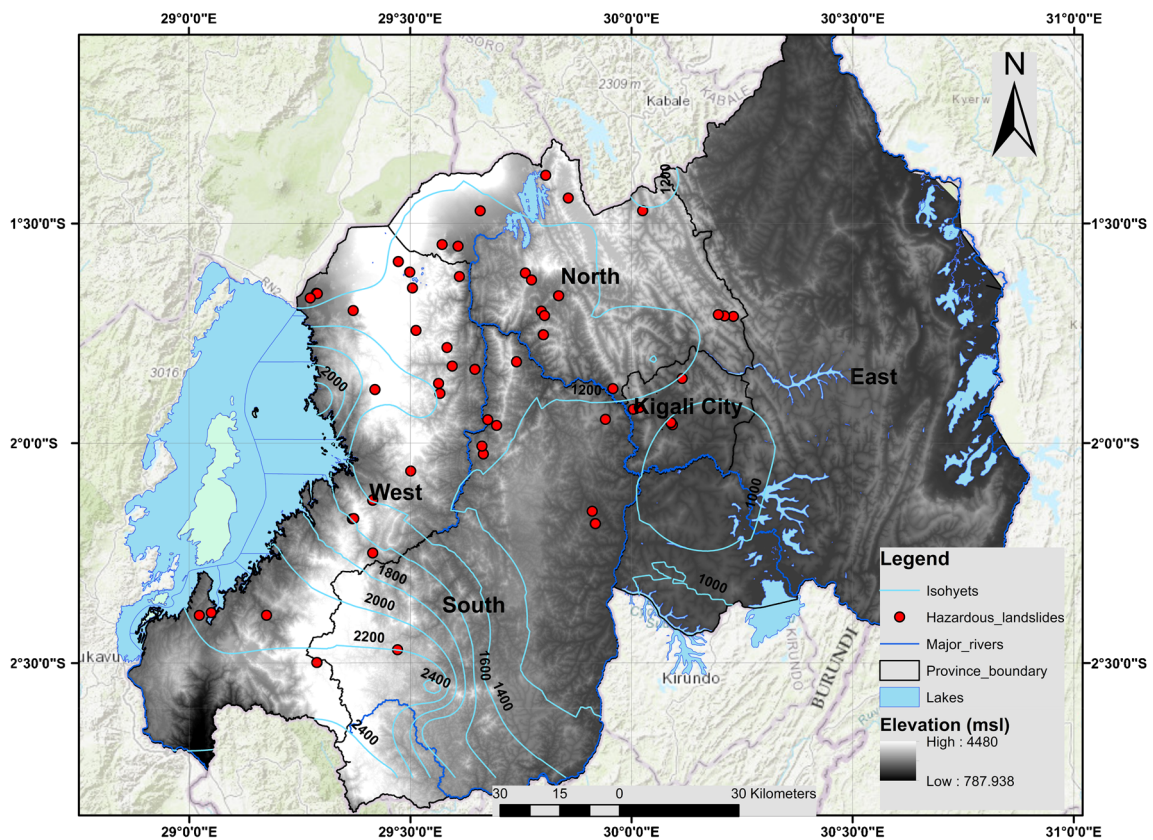
Fig. 2 Elevation map of the study area, isohyets (mm) and recorded landslides from 2006 to 2018 (red dots)
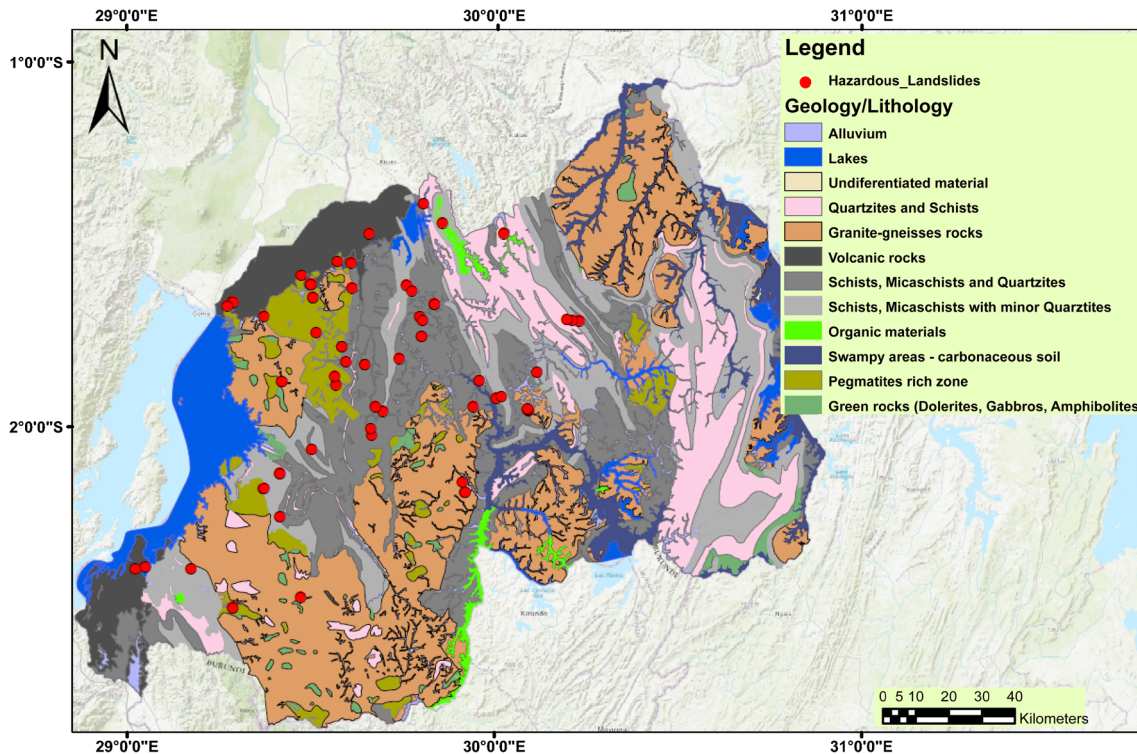
Fig. 3 Geology and lithological units of Rwanda and landslides (red dots) distribution

Landslides inventory
Part of the landslide inventory for Rwanda was accessed from the NASA global landslide catalogue (https://data.nasa.gov/Earth-Science/Global-Landslide-Catalog/h9d8-neg4) uploaded mainly by the LIWEAR project. The catalogue was extended through compilation of other rainfall-induced landslides as reported from local newspapers, blogs, technical reports and field observations. For the catalogue extension, we followed the global landslide inventory methods using standard indices adopted by Kirschbaum et al. (2012), Bach et al. (2010) and Monsieurs et al. (2018c). Seven elements were recorded for each landslide: (i) Landslide location (e.g. Village, cell, sector, district or town); (ii) time of occurrence (date); (iii) triggering event (e.g. rainfall); (vi) landslide type based on Hungr et al. (2014) classification and depending on the availability of background information; (v) latitude and longitude with relative locational accuracy; (vi) information about the impact (number of fatalities, injuries and damages); (vii) the accessible source of information was also mentioned with links to online source of information. Only hazardous (fatal and highly damaging) landslides are mostly reported while non-hazardous ones are likely to be missed. Based on the inventory, about 99% of landslides occurred from 2006 while the remaining occurred far before 2006. Therefore, 2006 was taken as the threshold year and landslides that occurred between 2006 and 2018 were used for this study.

Rainfall and representative rain gauges
We used daily rainfall time series recorded from 35 rain gauges in Rwanda over a period of 13 years from 2006 to 2018. The rainfall dataset was accessed from Rwanda Meteorology Agency. Among the 35 rain gauges, representative rain gauges were selected to

identify the rainfall conditions for each or multiple landslide. The representative rain gauges were selected based on their weights (W) estimated based on the cumulated rainfall event (E) until the landslide day, the distance between rain gauge and landslide (d) and duration D (days) firstly proposed by Melillo et al. (2018) using Eq. (1).

$$W = \frac{E^2}{d^2 D} \tag{1}$$

The number of rain gauges to be weighted for each landslide was chosen based on their location inside the buffer radius around the landslide location. The higher the weight, the higher the chance for the rain gauge to represent the rainfall conditions responsible for the landslide. Based on the highest weights (W) proposed by Melillo et al. (2018), 22 rain gauges out of 35 were found to be representative for the rainfall conditions responsible for the landslide occurrence. A single dataset of rainfall conditions from 22 rain gauges was made to pinpoint the landslide triggering conditions from non-triggering conditions.

Methodology

Definition of landslide rainfall conditions
The landslide conditions were divided into 4 categories based on their timescale. The first category considers the entire rainfall event during which one or more landslides occurred and is referred as the maximum probable rainfall event (MPRE). The second, third and fourth categories respectively consider the accumulation of very recent rainfall over the last 3 days (RD_3), 2 days (RD_2) and 1 day (RD_1) with the last day coinciding with the day of landslide occurrence. The RD_3, RD_2 and RD_1 for each day

during the 2006–2018 study period were calculated, irrespective of a landslide occurring or not. MPRE was here defined as individual periods of days with recorded rain ≥ 1 mm day^{-1} interrupted by dry periods of at least two dry days. The rainfall event E (mm/E) was then computed as the accumulated rainfall during each MPRE which is equivalent to the event duration D (day). The event intensity (mm day^{-1}) was then computed as a ratio of E and D. Landslide causal conditions were represented by the Antecedent Precipitation Index (API) considered as a proxy for soil moisture accumulation. The API was calculated as a cumulative rainfall occurring over a predefined time periods prior to the landslide triggering conditions. For this study, time periods of $T = 30$, 10 and 5 days were considered to define the API$_{30}$, API$_{10}$ and API$_5$, respectively. A decay coefficient $k = 0.95$ was used to estimate API$_T(t)$ for each day t over the study period according to the Eq. (2).

$$\text{API}_T(t) = R(t) + kR(t-1) + k^2 R(t-2) + k^3 R(t-3) \cdots \cdots R(t-T) \quad (2)$$

where R is the daily rainfall (mm day^{-1}), k is the decay coefficient (−), t is the individual day and T is the antecedent accumulation period (day) (30, 10 and 5 days) prior to the starting day of the rainfall triggering conditions (MPRE, RD$_3$, RD$_2$ and RD$_1$).

Quantification of landslide explanatory precipitation variables

The landslide explanatory precipitation variables which include the landslide causal (pre-disposing) and triggering conditions were explored using receiver operating characteristic (ROC) curves (Hong et al. 2017; Postance and Hillier 2017; Mirus et al. 2018a; Prenner et al. 2018). The ROC is a graphical representation created by plotting the false positive rate (FPR) of wrongly predicted landslides against the true positive rate (TPR) of correctly predicted landslides. The ROC curves are made of a suite of possible threshold levels at which a balance between each threshold's true positive rate and the corresponding false positive rate is evaluated. The area under the ROC curve (AUC) is used as an indicator of the variable performance, where a perfect test variable would result in an AUC = 1. The AUC indicates the capacity of the considered test variable to correctly distinguish landslide from no-landslide conditions. Thus, the AUC was used on the one hand as a statistical metric to compare the tested precipitation variables against random guessing, i.e. AUC = 0.5. On the other hand, it was used to find precipitation-related variable with the highest explanatory power for landslide. The true positive rate (TPR) associated with each threshold level on ROC curves is calculated with Eq. (3).

$$\text{TPR} = \frac{\text{TP}}{\text{TP} + \text{FN}} \quad (3)$$

The false positive rate (FPR) is calculated by Eq. (4).

$$\text{FPR} = \frac{\text{FP}}{\text{FP} + \text{TN}} \quad (4)$$

where TP are true positives, i.e. the number of landslides correctly predicted by the threshold; FN are false negatives, and thus the number of landslides that occurred in reality but that were not predicted, i.e. the number of landslide triggered by rainfall conditions below the defined threshold. FP are false positives, i.e. incorrect predictions of landslide occurrence by the threshold model while in reality, there was no landslide reported. TN are true negatives, i.e. are correct predictions of no landslide occurring.

Threshold definition techniques

Since the AUC only indicate which precipitation variable or combination of variables that can significantly distinguish landslide from no landslide and the ROC curves indicating all possible thresholds and their respective balance of TPR and FPR, it is also necessary to define the optimum threshold levels above which landslide are high likely to occur. We used 3 different techniques to do that: Bayesian probabilistic approach (Prob), maximum true skill statistic (TSS) and minimum radial distance (Rad). The Bayes' theorem defines the conditional probability of an event A (here: landslide occurrence) given an event B, here represented by different precipitation variables as introduced in the "Definition of landslide rainfall conditions" section. To reduce the high rainfall data scattering, specific magnitude-frequency distributions for each rainfall variable were defined using bins. Based on the extent of the dataset, bins of 5 mm were used for E, RD and API while 2 mm day^{-1} and 2 days were used for event intensity and event duration respectively. The specific magnitude-frequency pairs were then converted into probabilities based on Bayes' terminologies. The Bayes' prior probability of an event A, $P(A)$ stands for the global probability of landslide to occur regardless of the event B. If N_{A_T} denotes the total number of landslide conditions ($\approx$ total number of landslides) and N_{B_T} the total number of rainfall events (landslide + no landslide conditions) recorded over the predefined period (here 2006–2018), $P(A)$ is calculated with Eq. (5).

$$P(A) = \frac{N_{A_T}}{N_{B_T}} \quad (5)$$

If we define also N_{B_S} as the number of events B with specific magnitude (e.g. 20 mm $\leq E <$ 25 mm), the prior probability for an event B denoted as $P(B)$ is thus expressed with Eq. (6) and indicates the probability to have an event B regardless of whether landslide occurs or not.

$$P(B) = \frac{N_{B_S}}{N_{B_T}} \quad (6)$$

The conditional probability $P(A|B)$ expressed in Eq. (7) indicates the probability for landslide occurrence given the specific magnitude of rainfall variable.

$$P(A|B) = \frac{P(B|A) \cdot P(A)}{P(B)} \quad (7)$$

The conditional probability $P(B|A)$ is the probability to have rainfall of a specific magnitude B_S given that landslide occurs and is calculated by Eq. (8) or (9).

$$P(B|A) = \frac{P(B) \cdot P(A|B)}{P(A)} \quad (8)$$

$$P(B|A) = \frac{N_{A_S}}{N_{A_T}} \quad (9)$$

Cum P: Cumulative Probability   A: Landslide   B: Intensity
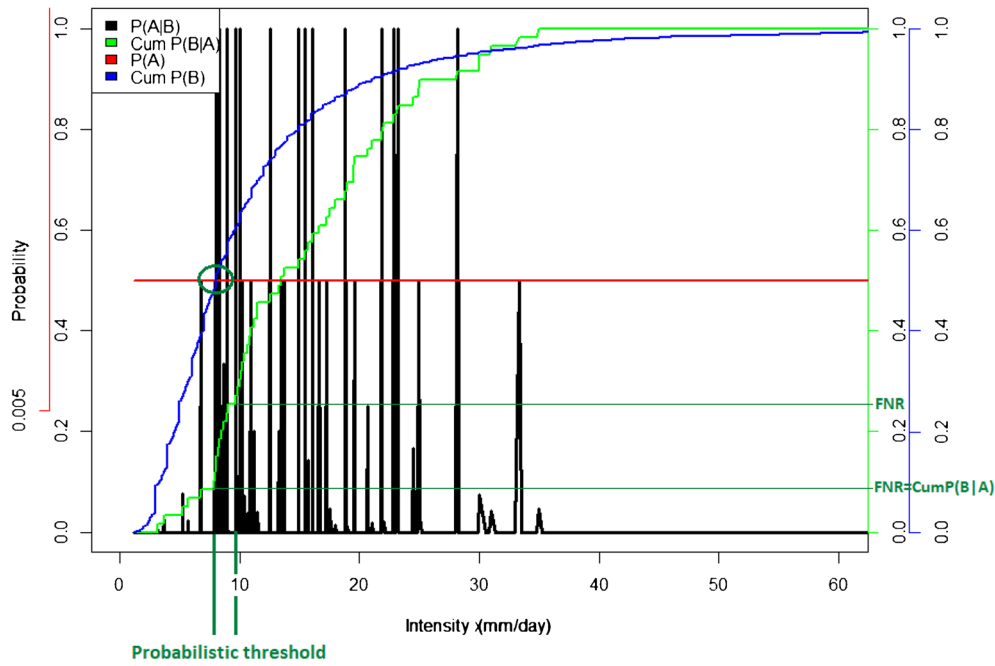
Fig. 4 Probabilistic threshold definition: on X axis is the magnitude of event intensity I; on Y primary axis: the red constant curve is the prior landslide probability $P(A)$; the black axis represents the conditional probability to have landslide given a specific magnitude of I ($P(A|B)$). On secondary Y axis: the light green axis is the cumulative probability to have an event intensity I of specific magnitude given that landslide occurs $cumP(B|A)$; the blue axis represents the cumulative probability of I regardless of landslide occurrence or not ($cumP(B)$). The dark green sphere and 2 vertical lines indicate the specific magnitude or level at which $P(A|B)$ goes beyond $P(A)$ and this represents the probabilistic threshold intensity which is between 8 and 10 mm day^{-1}. The dark green horizontal lines indicate the resulting false negative rate equivalent to the Cum $P(B|A)$ represented by the light green curve

With N_{A_S} denoting the number of landslides that occur within a specific rainfall magnitude B_S (e.g. number of landslide that occurs when rainfall intensity was between 8 and 10 mm day^{-1} $8 \leq I < 10$), the probabilistic threshold values are defined by comparing the prior $P(A)$ to the posterior probability $P(A|B)$ (Berti et al. 2012; Robbins 2016; Peres et al. 2017). If the posterior landslide probabilities $P(A|B)$ differ from the prior landslide probability $P(A)$, the rainfall variable (B) has a significant effect on landslide occurrence (A). Contrary, when $P(A|B)$ is objectively smaller or equal to $P(A)$, there is no significant effect of variable B. The probabilistic threshold value for a variable B to initiate landslide (A) is objectively taken as the specific magnitude or level at which the posterior probability distribution curve $P(A|B)$ goes beyond the prior probability distribution curve of $P(A)$ as shown on Fig. 4. The cumulative probability curve $cumP(B|A)$ indicates the probability to have landslides below and above the threshold level of B, respectively. This is equivalent to the false negative (FNR) and true positive rates (TPR) on the ROC curve as expressed by Eqs. (10)–(12).

$$\text{FNR} = cumP(B|A) \qquad (10)$$

or

$$\text{FNR} = \frac{\text{FN}}{\text{FN} + \text{TP}} \qquad (11)$$

$$\text{TPR} = 1 - cumP(B|A) \qquad (12)$$

The threshold definition based on the maximum true skill statistics TSS (e.g. Ciavolella et al. 2016; Peres et al. 2017) and the minimum radial distance Rad (Postance and Hillier 2017; Mirus et al. 2018a) has been particularly used in landslide studies. The true skill statistics is expressed as a balance between the true positive rate and false positive rate as indicated on Eq. (13) and its maximum value indicates the optimum threshold. For a perfect threshold, the TSS would be a unity, i.e. with zero false positive rate. On the ROC curve, the radial distance (Eq. (14)) indicates the relative distance from the defined threshold to the optimum point whose TPR is a unit and FPR is zero. Thus, the minimum radial distance would be zero for a perfect threshold (Postance and Hillier 2017).

$$\text{TSS} = \text{TPR} - \text{FPR} \qquad (13)$$

$$\text{Rad} = \sqrt{\text{FPR}^2 + (\text{TPR} - 1)^2} \qquad (14)$$
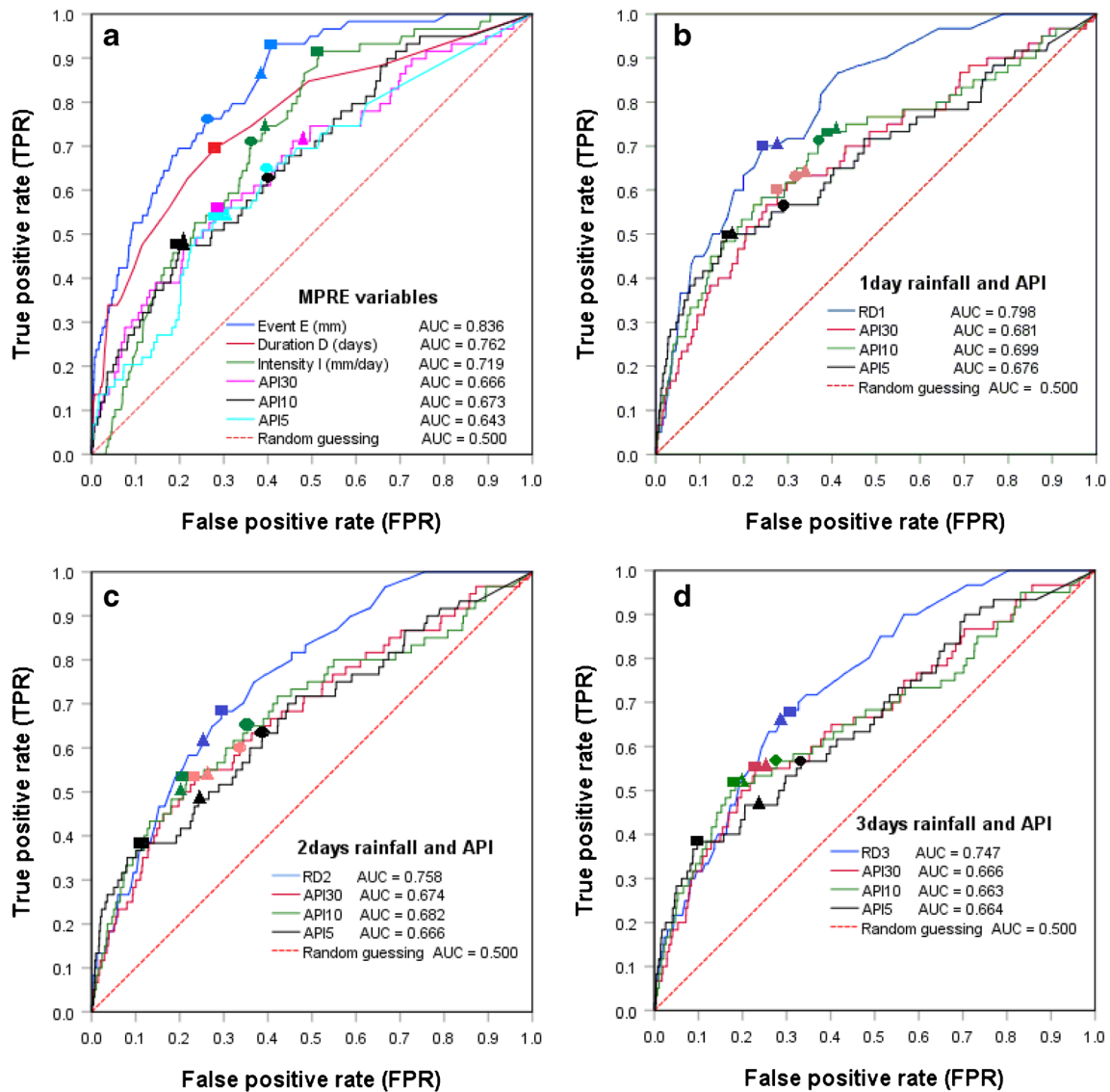
Fig. 5 Receiver operating characteristic (ROC) curves for **a** MPRE variables, **b** RD1 variables, **c** RD2 variables and **d** RD3 variables; variable significance based on the area under the curve (AUC) and the optimum thresholds defined using Bayesian probabilistic approach (triangle shaped marker); maximum true skill statistics (rectangle-shaped marker) and the minimum radial distance (sphere-shaped marker). Once two or more techniques revealed similar threshold with similar TPR and FPR, only one symbol is used. The figure also indicates corresponding true positive rate (TPR) and false positive rate (FPR) for each threshold level

Cause-trigger-based thresholds definition and implication for landslide prediction

The cause-trigger-based thresholds were defined by combining the best performing thresholds selected from one of the techniques described in the "Threshold definition techniques" section. According to Postance and Hillier (2017), the ideal landslide warning threshold is the one leading to the maximum positive alarms (TP), minimum failed alarms (FN) and also with minimum number of false alarms (FP). Based on these criteria, the most realistic threshold was selected among the ones defined either by Bayesian probabilistic approach, maximum true skill statistics or minimum radial distance. These thresholds were plotted on both axis of landslide triggering and causal variables in Y, X pairs as I-API_{30}, I-API_{10}, I-API_5, E-API_{30}, E-API_{10}, E-API_5, RD_1-API_{30}, RD_1-API_{10}, RD_1-API_5, RD_2-API_{30}, RD_2-API_{10}, RD_2-API_5, RD_3-API_{30}, RD_3-API_{10} and RD_3-API_5. To evaluate the performance of the newly

adopted method, a confusion matrix for each pair was performed and the resulting rate of positive alarms, false alarms, failed alarms and true negatives was quantified.

Results and discussion

Landslide explanatory rainfall variables and thresholds

A total number of 9353 MPRE from 34,438 rainy days (RD) that include landslide and no landslide conditions were recorded in Rwanda from 2006 to 2018. From this MPRE and RD catalogue, 59 MPRE and 60 RD (≈ total number of landslides) were highlighted as conditions responsible for the occurrence of one or more landslides recorded in the inventory. The area under the curve (AUC) of each variable of the MPRE and RD in Fig. 5 indicated the probability of all test variables to correctly distinguish landslide from no-landslide conditions. The AUC was highest for entire rainfall events

Table 1 MPRE landslide explanatory precipitation variables and their thresholds defined using probabilistic approach (Prob), maximum true skill statistics (TSS) and minimum radial distance (Rad)

Variables	Bayesian probabilistic threshold[P]			Maximum True skill statistics (TSS)				
	Threshold	$1-P(BA)$/TPR	FPR	Threshold	TSS	Rad	TPR	FPR
1. Trigger-based thresholds								
Event E (mm E^{-1})	32.5	0.847	0.376	29.95	0.472	0.406	0.932	0.409
Intensity (mm day^{-1})	9.00	0.746	0.419	7.87	0.327	0.490	0.915	0.517
Duration (days)	4.00	0.695	0.279	4.50	0.415	0.414	0.695	0.279
2. Cause-based thresholds								
API_{30} (mm)	47.50	0.712	0.485	66.81	0.227	0.564	0.559	0.286
API_{10} (mm)	37.50	0.475	0.201	37.73	0.273	0.563	0.475	0.199
API_{5} (mm)	12.50	0.542	0.283	12.49	0.260	0.538	0.542	0.283

Variables	Maximum True skill statistics (TSS)		Minimum radial distance (Rad)				
	TSS	Rad	Threshold	TSS	Rad	TPR	FPR
1. Trigger-based thresholds							
Event E (mm E^{-1})	0.523	0.415	45.90	0.501	0.353	0.763	0.262
Intensity (mm day^{-1})	0.399	0.524	10.05	0.350	0.463	0.712	0.362
Duration (days)	0.415	0.414	4.50	0.415	0.414	0.695	0.279
2. Cause-based thresholds							
API_{30} (mm)	0.273	0.526	66.81	0.273	0.526	0.559	0.286
API_{10} (mm)	0.276	0.562	23.57	0.228	0.546	0.627	0.399
API_{5} (mm)	0.260	0.538	7.65	0.247	0.534	0.644	0.398

[P] The probabilistic threshold is a mean value from different probabilistic range, for example a threshold value of 32.5 is a mean value ranging between 30 and 35 and a threshold value of 27.5 is a mean value between 25 and 30

Table 2 Cumulative recent rainfall variables (RD$_1$, RD$_2$, RD$_3$), antecedent precipitation index (API) and landslide initiation thresholds defined using probabilistic (Prob), maximum true skill statistics (TSS) and the minimum radial distance (Rad) techniques

Variable	Bayesian probabilistic threshold (Prob)[p]					Maximum True skill statistics (TSS)		
	Threshold	1-P(B\A)/TPR	FPR	TSS	Rad	Threshold	TPR	FPR
1. Trigger-based thresholds								
RD$_1$ (mm day^{-1})	12.50	0.717	0.298	0.418	0.411	14.45	0.700	0.245
RD$_2$ (mm day^{-2})	22.50	0.617	0.257	0.360	0.461	22.05	0.617	0.258
RD$_3$ (mm)	27.50	0.667	0.291	0.376	0.442	26.95	0.683	0.307
2. Cause-based thresholds								
API$_{30}$ (mm)[a]	92.50	0.633	0.320	0.487	0.313	99.08	0.600	0.277
API$_{10}$ (mm)[a]	42.50	0.733	0.408	0.326	0.487	44.37	0.733	0.385
API$_5$ (mm)[a]	42.50	0.500	0.173	0.327	0.529	44.04	0.500	0.160
API$_{30}$ (mm)[b]	102.50	0.533	0.250	0.283	0.529	105.34	0.533	0.235
API$_{10}$ (mm)[b]	62.50	0.517	0.202	0.315	0.524	61.05	0.533	0.215
API$_5$ (mm)[b]	32.50	0.483	0.263	0.220	0.580	49.51	0.383	0.113
API$_{30}$ (mm)[c]	102.50	0.550	0.248	0.302	0.514	105.79	0.550	0.229
API$_{10}$ (mm)[c]	62.50	0.517	0.202	0.315	0.524	65.01	0.517	0.184
API$_5$ (mm)[c]	32.50	0.467	0.258	0.209	0.592	52.16	0.383	0.097

Variable	Maximum True skill statistics (TSS)		Minimum radial distance (Rad)				
	TSS	Rad	Threshold	TPR	FPR	TSS	Rad
1. Trigger-based thresholds							
RD$_1$ (mm day^{-1})	0.455	0.387	14.45	0.700	0.245	0.455	0.387
RD$_2$ (mm day^{-2})	0.359	0.462	20.85	0.683	0.295	0.389	0.432
RD$_3$ (mm)	0.376	0.441	26.95	0.683	0.307	0.376	0.441
2. Cause-based thresholds							
API$_{30}$ (mm)[a]	0.323	0.487	92.97	0.633	0.317	0.317	0.484
API$_{10}$ (mm)[a]	0.349	0.468	45.58	0.717	0.371	0.346	0.466
API$_5$ (mm)[a]	0.340	0.525	31.79	0.567	0.290	0.277	0.521
API$_{30}$ (mm)[b]	0.299	0.522	88.02	0.617	0.344	0.273	0.515
API$_{10}$ (mm)[b]	0.318	0.514	45.87	0.650	0.354	0.296	0.498
API$_5$ (mm)[b]	0.270	0.627	24.57	0.633	0.387	0.247	0.533
API$_{30}$ (mm)[c]	0.321	0.505	105.79	0.550	0.229	0.321	0.505
API$_{10}$ (mm)[c]	0.333	0.517	53.22	0.567	0.278	0.289	0.515

Table 2 (continued)

| Variable	Maximum True skill statistics (TSS)		Minimum radial distance (Rad) Threshold	TPR	FPR	TSS	Rad
	TSS	Rad					
API_5 (mm)[c]	0.286	0.624	27.31	0.567	0.332	0.234	0.546

[p] The probabilistic threshold is a mean value from different probabilistic range, for example a threshold value of 32.5 is a mean value ranging between 30 and 35 and a threshold value of 27.5 is a mean value between 25 and 30

[a] 30-, 10- and 5-day antecedent precipitation index prior to 1 day triggering rainfall coinciding with landslide day

[b] 30-, 10- and 5-day antecedent precipitation index prior to 2 days triggering rainfall whose last day coincides with landslide day

[c] 30-, 10- and 5-day antecedent precipitation index prior to 3 days triggering rainfall whose last day coincides with landslide day

E and the cumulated 1-day rainfall RD_1 as compared with other landslide triggering precipitation variables. This suggests that in the study region the cumulated rainfall received on the day of a landslide has more impact to trigger landslides than previously recorded rainfall. It also indicates that shorter timescale triggering conditions are more relevant for landslide occurrence than longer timescales. Even though, rainfall event volumes E have also scored higher at distinguishing landslide from no-landslide conditions, it is critical to note that E has variable timescales that should be normalised by the event duration D and thus ending up with event intensity I as the most informative test variable. The overall performance of antecedent precipitation indices (API), here considered as landslide cause, indicates that the cumulated rainfall over 10 days (API_{10}) prior to the landslide triggering conditions has the most influential effect on landslide occurrence as compared with longer (30 days) and shorter (5 days) antecedent periods. On the one hand, this can be attributed to the hydro-geotechnical properties of soil-like hydraulic conductivity, permeability and soil texture that contribute to subsequent interplay between infiltration, evaporation and drainage and thus the drawdown of the longer antecedent precipitation (API_{30}) period. On the other hand, this may indicate the lags in water flow to reach the critical layer of the regolith for shorter periods like API_5. The ROC curves in Fig. 5 indicate the possible threshold levels for each tested variable and the respective balance of TPR and FPR. The optimum threshold levels above which landslide is high likely to occur are presented with different symbols on the curve depending on the technique used. The detailed information of the defined optimum thresholds is summarised in Table 1. The maximum true skill statistics (TSS) indicated that landslide is high likely to occur when the cumulated rainfall volume E goes beyond 29.9 mm/E and this threshold level resulted to about 93% of correct predictions of landslide, i.e. true positive alarms and about 41% of false alarms. A similar threshold was obtained based on Prob, indicating the highest probability for landslides to occur beyond 30–35 mm/E with a mean value of 32.5 mm/E. However, the minimum radial distance (Rad) approach revealed a higher threshold level of about 45.9 mm/E associated with quite lower positive alarms (76.3%) in favour of a lower rate of false alarms (26.2%). From TSS, Prob and Rad, the critical event duration was inferred to be around 4 days which would lead to the normalised event E_n thresholds of about 7.5 mm day^{-1}, 8.1 mm day^{-1} and 11.5 mm day^{-1} respectively. These thresholds are similar to the defined event intensity thresholds of 7.9 mm day^{-1}, between 8 and 10 mm day^{-1} and 10.1 mm day^{-1} respectively from TSS, Prob and Rad. Based on daily rainfall (RD) variables in Table 2, the optimum threshold levels above which landslide are high likely to occur were 12.5 mm day^{-1}(Prob), 20.9 mm day^{-2} (Rad) and 27.0 mm day^{-3} (TSS and Rad) for RD_1, RD_2 and RD_3 respectively. The optimum API threshold levels were also defined as indicated on Fig. 4 and Tables 1 and 2. The most informative thresholds were 45.5 mm (Prob), 23.6 mm (Rad) and 7.7 mm (Rad) for API_{30}, API_{10} and API_5 respectively prior to the landslide triggering event (MPRE). The API thresholds for RD variables are also presented in Table 2. It has to be understood that the API thresholds indicate the levels below which no influence of antecedent precipitation would be expected to contribute to the landslide triggering conditions. However, it has to be noted that API thresholds are very sensitive to the timescale of the triggering conditions. Shorter timescale triggering conditions like RD_1require higher threshold levels of API as compared
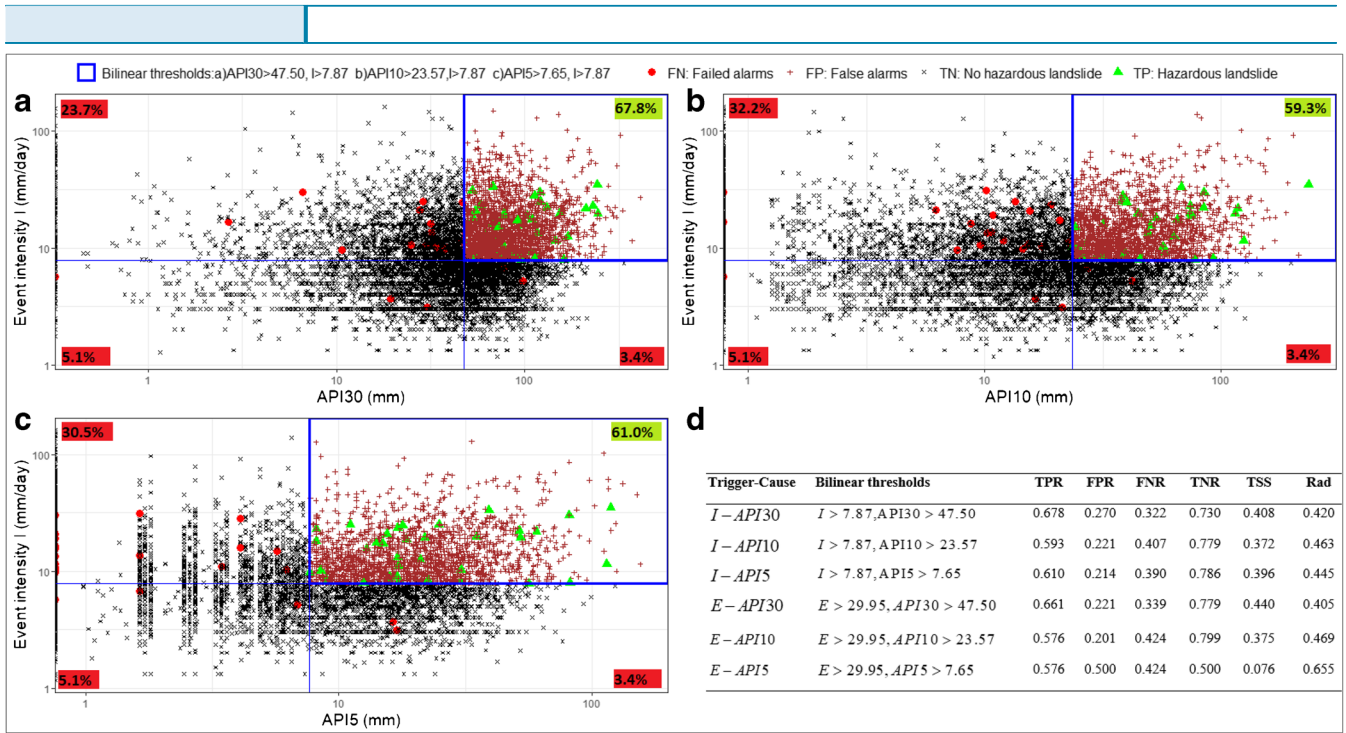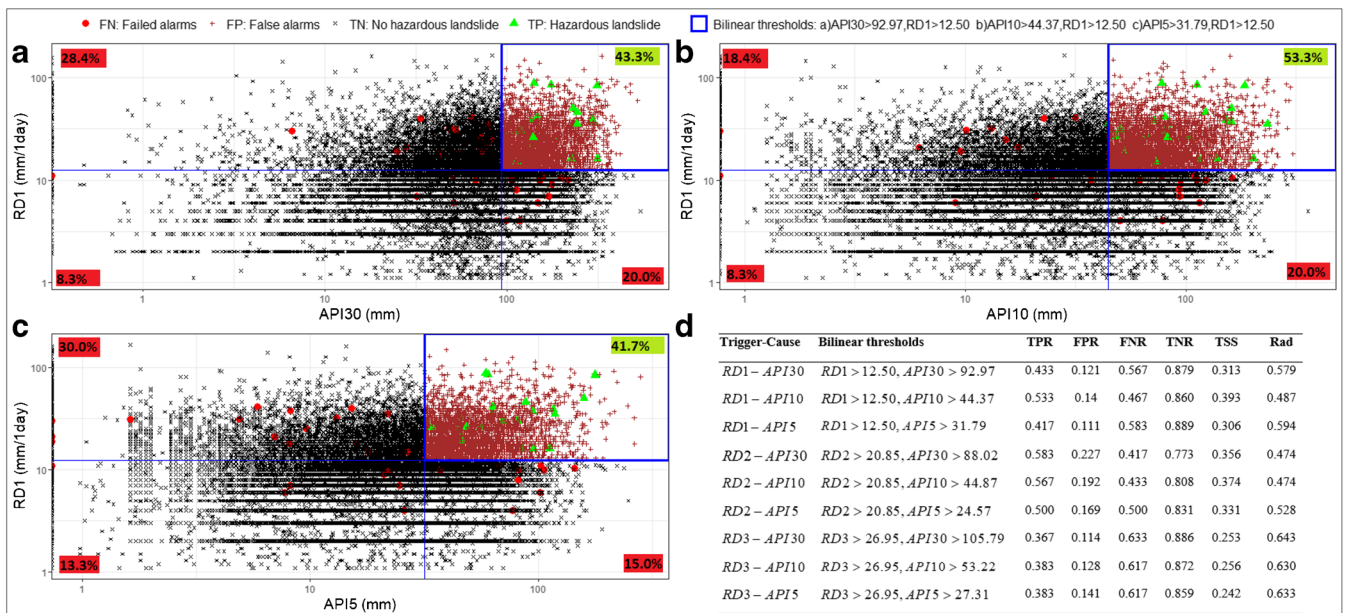
Fig. 6 Bilinear relation between landslide trigger represented by event intensity I and cause represented by antecedent precipitation indices of different timescales. **a** Thirty days prior to the triggering event intensity. **b** Ten days prior to the triggering event intensity. **c** Five days prior to the triggering event intensity. **d** Implication for warning based on the rate of true warnings (TPR) represented by green triangles on **a**, **b** and **c**; rate of false alarms (FPR) represented by red cross on **a**, **b** and **c**; rate of failed alarms (FNR) represented by red dots on **a**, **b** and **c**; true negative rate (TNR) or no landslide represented by black cross on **a**, **b** and **c**

Trigger-Cause	Bilinear thresholds	TPR	FPR	FNR	TNR	TSS	Rad
$I-API30$	$I > 7.87, API30 > 47.50$	0.678	0.270	0.322	0.730	0.408	0.420
$I-API10$	$I > 7.87, API10 > 23.57$	0.593	0.221	0.407	0.779	0.372	0.463
$I-API5$	$I > 7.87, API5 > 7.65$	0.610	0.214	0.390	0.786	0.396	0.445
$E-API30$	$E > 29.95, API30 > 47.50$	0.661	0.221	0.339	0.779	0.440	0.405
$E-API10$	$E > 29.95, API10 > 23.57$	0.576	0.201	0.424	0.799	0.375	0.469
$E-API5$	$E > 29.95, API5 > 7.65$	0.576	0.500	0.424	0.500	0.076	0.655

with RD_2 or MPRE. This shows that relying on trigger-based thresholds for landslide early warning could lead to biased results rather than relying more on API's thresholds. Thus, shorter timescale triggering conditions should be preferred as confirmed based on AUC.

Landslide trigger and trigger-cause-based thresholds and implication for landslide prediction

The results of bilinear combinations of explanatory variables show that in some cases, a single variable threshold can be sufficient to predict landslides (Figs. 6 and 7), horizontal blue lines). Based on

Trigger-Cause	Bilinear thresholds	TPR	FPR	FNR	TNR	TSS	Rad
$RD1-API30$	$RD1 > 12.50, API30 > 92.97$	0.433	0.121	0.567	0.879	0.313	0.579
$RD1-API10$	$RD1 > 12.50, API10 > 44.37$	0.533	0.14	0.467	0.860	0.393	0.487
$RD1-API5$	$RD1 > 12.50, API5 > 31.79$	0.417	0.111	0.583	0.889	0.306	0.594
$RD2-API30$	$RD2 > 20.85, API30 > 88.02$	0.583	0.227	0.417	0.773	0.356	0.474
$RD2-API10$	$RD2 > 20.85, API10 > 44.87$	0.567	0.192	0.433	0.808	0.374	0.474
$RD2-API5$	$RD2 > 20.85, API5 > 24.57$	0.500	0.169	0.500	0.831	0.331	0.528
$RD3-API30$	$RD3 > 26.95, API30 > 105.79$	0.367	0.114	0.633	0.886	0.253	0.643
$RD3-API10$	$RD3 > 26.95, API10 > 53.22$	0.383	0.128	0.617	0.872	0.256	0.630
$RD3-API5$	$RD3 > 26.95, API5 > 27.31$	0.383	0.141	0.617	0.859	0.242	0.633

Fig. 7 Bilinear relation between landslide trigger represented by 1-day rainfall (RD_1) and cause represented by antecedent precipitation indices (API) of different timescales. **a** Thirty days prior to the triggering rainfall. **b** Ten days prior to the triggering rainfall. **c** Five days prior to the triggering rainfall. **d** Implication for warning based on the rate of true warnings (TPR) represented by green triangles on **a**, **b** and **c**; rate of false alarms (FPR) represented by red cross on **a**, **b** and **c**; rate of failed alarms (FNR) represented by red dots on **a**, **b** and **c**; true negative rate (TNR) or no landslide represented by black cross on **a**, **b** and **c**

the maximum TSS threshold (Fig. 5, Tables 1 and 2), 91.5% of the landslides are correctly predicted once an event intensity threshold level of 7.9 mm day^{-1} is exceeded. Similarly, 93.5% of the landslides are highly likely to occur when the rainfall event E exceeds 30.0 mm while 71.7% of the landslides are highly likely to occur when daily rainfall (RD$_1$) exceeds 12.5 mm day^{-1}. These threshold levels are all trigger-based as they only refer to the recent rainfall/event during which one or more landslides occur. However, these trigger-based thresholds should be constrained by relatively high rates of false alarm (FPR) of about 52%, 41% and 30% for I, E and RD$_1$ respectively. Moreover, it should be noted that many landslides occur not only due to the trigger itself but rather due to a combination of trigger and cause, the latter represented by API. For example in Fig. 6a, it can be seen that only 23.7% of the observed landslides, which is equivalent to about 26% of the correctly predicted landslides using event intensity (I) threshold, was due to the triggering event while the remaining 74% of the predicted landslides were due to the combined effect of both I and API. As pointed out in the "Landslide explanatory rainfall variables and thresholds" section, the API thresholds indicate the critical level below which the impact of antecedent precipitation is considered unimportant for landslide predictions. On the contrary, once the API threshold is exceeded, its contribution should be counted as one of the landslide causal factor and thus resulting into trigger-cause-based thresholds. The top left and right panels of Figs. 6 and 7 indicate the improved prediction capacity of the trigger-based threshold once combined with a cause-based threshold. For example Fig. 6 indicates that the prediction capacity (TPR) of the event intensity threshold increased by about 44%, 27% and 30% once combined with API as trigger-cause-based thresholds in a bilinear format as I-API$_{30}$, I-API$_{10}$ and I-API$_5$ respectively. Figure 7 indicates also an improved prediction rate of RD$_1$ trigger-based threshold by about 15%, 35% and 12% once combined as RD$_1$-API$_{30}$, RD$_1$-API$_{10}$ and RD$_1$-API$_5$ respectively. Therefore, the concept of bilinear thresholds (Mirus et al. 2018a) or trigger-cause-based thresholds does not only minimise the false alarm rates but can also be utilised to quantify the impact of each and both landslide triggering and causal condition to the landslide occurrence. Figures 6 and 7 show the resulting rate of true alarms (TPR), false alarms (FPR), failed alarms (FNR) and true negative rate (TNR) from different trigger-cause-based thresholds. This approach should further be explored to be utilised for API-based landslide early warning system development.

Lastly, as pointed out in the introductory part of this article, the landslide inventory used for this research relied largely on the information from newspapers, government reports and other media where many landslide events are likely to be missed. While the reliance on these data sources is likely to result in a bias towards large and/or impactful landslides that may involve casualties and economic damage, this landslide inventory is the most comprehensive currently available in Rwanda.

Conclusion

This research aimed to use landslide and precipitation data in an empirical-statistical approach to define both trigger and trigger-cause-based thresholds for landslide initiation in Rwanda and to quantify their predictive performance. The findings of this study indicated that the normalised event E and the cumulative 1-day rainfall (RD$_1$) that coincide with the landslide day are the most informative explanatory variables to distinguish landslide from no landslide conditions. Among the antecedent precipitation indices, 10-day rainfall prior to the landslide triggering conditions was the most informative to distinguish between landslide and no-landslide conditions based on its AUC. API$_5$ was too short while API$_{30}$ was too long. This underlines the critical role of hydrology (infiltration, storage, evaporation/drainage) and particularly the timing of pore pressure changes in the subsurface profile. It was also generally observed that all used threshold definition techniques, Bayesian probabilistic approach, maximum true skill statistic and minimum radial distance, resulted in quite similar threshold values. The highest landslide prediction capability (rate of positive alarms) was obtained using a single rainfall variable, so a trigger-based threshold. However, that predictive capability simultaneously resulted in a high rate of false alarms. Constraining the trigger-based threshold with a causal variable in a bi-linear framework as proposed by Mirus et al. 2018a improved the overall prediction capacity by reducing the number of false alarms. The findings indicated also that the concept of trigger-cause-based thresholds in bilinear format could not only be useful to minimise the false alarms but also to explore the impact of each or combined triggering and causal conditions on landslide occurrence.

References

Aleotti P (2004) A warning system for rainfall-induced shallow failures. Eng Geol 73:247–265. https://doi.org/10.1016/j.enggeo.2004.01.007

Anderson MG, Lloyd DM (1991) Using a combined slope hydrology- stability model to develop cut slope design charts. ICE Proc 91:705–718. https://doi.org/10.1680/iicep.1991.17486

Bach D, Ae K, Adler R, et al (2010) A global landslide catalog for hazard applications: method, results, and limitations. 52:561–575. https://doi.org/10.1007/s11069-009-9401-4

Berti M, Martina MLV, Franceschini S, et al (2012) Probabilistic rainfall thresholds for landslide occurrence using a Bayesian approach. J Geophys Res Earth Surf 117:n/a-n/a. https://doi.org/10.1029/2012JF002367

Bogaard T, Greco R (2018) Invited perspectives: hydrological perspectives on precipitation intensity-duration thresholds for landslide initiation: proposing hydro-meteorological thresholds. Nat Hazards Earth Syst Sci 18:31–39. https://doi.org/10.5194/nhess-18-31-2018

Caine N (1980) The rainfall intensity : duration control of shallow landslides and debris flows. JSTOR 62:23–27

Ciavolella M, Bogaard T, Gargano R, Greco R (2016) Is there predictive power in hydrological catchment information for regional landslide Hazard assessment? Procedia Earth Planet Sci 16:195–203. https://doi.org/10.1016/j.proeps.2016.10.021

Crozier MJ (1999) Prediction of rainfall-triggered landslides : a test of the antecedent water status model. Earth Surf Process Landforms 833:825–833

Dewitte O, Jones A, Spaargaren O, Breuning-Madsen H, Brossard M, Dampha A, Deckers J, Gallali T, Hallett S, Jones R, Kilasara M, le Roux P, Michéli E, Montanarella L, Thiombiano L, van Ranst E, Yemefack M, Zougmore R (2013) Harmonisation of the soil map of africa at the continental scale. Geoderma 211–212:138–153. https://doi.org/10.1016/j.geoderma.2013.07.007

Froude MJ, Petley DN (2018) Global fatal landslide occurrence from 2004 to 2016. Nat Hazards Earth Syst Sci 18:2161–2181. https://doi.org/10.5194/nhess-18-2161-2018

Gariano SL, Guzzetti F (2016) Landslides in a changing climate. Earth-Science Rev 162:227–252. https://doi.org/10.1016/J.EARSCIREV.2016.08.011

Glade T (2000) Modelling landslide-trigering rainfalls in different regions of New Zealand - the soil water status model. Geomorphology 122:63–84

Guzzetti F, Peruccacci S, Rossi M, Stark CP (2007) Rainfall thresholds for the initiation of landslides in central and southern Europe. Meteorog Atmos Phys 98:239–267. https://doi.org/10.1007/s00703-007-0262-7

Guzzetti F, Peruccacci S, Rossi M, Stark CP (2008) The rainfall intensity-duration control of shallow landslides and debris flows: an update. Landslides 5:3–17. https://doi.org/10.1007/s10346-007-0112-1

Hong M, Kim J, Jeong S (2017) Rainfall intensity-duration thresholds for landslide prediction in South Korea by considering the effects of antecedent rainfall. Landslides. https://doi.org/10.1007/s10346-017-0892-x

Hungr O, Leroueil S, Picarelli L (2014) The Varnes classification of landslide types, an update. Landslides 11:167–194. https://doi.org/10.1007/s10346-013-0436-y

Kirschbaum D, Adler R, Adler D, Peters-Lidard C, Huffman G (2012) Global distribution of extreme precipitation and high-impact landslides in 2010 relative to previous years. Hydrometeorology 3:1536–1551. https://doi.org/10.1175/JHM-D-12-02.1

Kuriakose SL, van Beek LPH, van Westen CJ (2009) Parameterizing a physically based shallow landslide model in a data poor region. Earth Surf Process Landforms 34:867–881. https://doi.org/10.1002/esp

Ma T, Li C, Lu Z, Bao Q (2015) Rainfall intensity–duration thresholds for the initiation of landslides in Zhejiang Province, China. Geomorphology 245:193–206. https://doi.org/10.1016/j.geomorph.2015.05.016

Melillo M, Brunetti MT, Peruccacci S, Gariano SL, Roccati A, Guzzetti F (2018) A tool for the automatic calculation of rainfall thresholds for landslide occurrence. Environ Model Softw 105:230–243. https://doi.org/10.1016/j.envsoft.2018.03.024

Mirus B, Morphew M, Smith J (2018a) Developing hydro-meteorological thresholds for shallow landslide initiation and early warning. Water 10:1274. https://doi.org/10.3390/w10091274

Mirus BB, Becker RE, Baum RL, Smith JB (2018b) Integrating real-time subsurface hydrologic monitoring with empirical rainfall thresholds to improve landslide early warning. Landslides 15:1909–1919. https://doi.org/10.1007/s10346-018-0995-z

Monsieurs E, Dewitte O, Demoulin A (2018a) A susceptibility-based rainfall threshold approach for landslide occurrence. Nat hazards earth Syst sci discuss 1–25. https://doi.org/10.5194/nhess-2018-316

Monsieurs E, Kirschbaum DB, Tan J, et al (2018b) Evaluating TMPA rainfall over the sparsely gauged East African Rift. J Hydrometeorol 19: https://doi.org/10.1175/JHM-D-18-0103.1

Monsieurs E, Liesbet J, Michellier C et al (2018c) Landslide inventory for hazard assessment in a data– poor context : a regional-scale approach in a tropical African environment. Landslides 10:100–2209. https://doi.org/10.1007/s10346-018-1008-y

Monsieurs E, Dewitte O, Depicker A, Demoulin A (2019) Towards a transferable antecedent rainfall—susceptibility threshold approach for landsliding. Water 2019, Vol 11, page 2202 11:2202. https://doi.org/10.3390/W11112202

Montgomery DR, Dietrich WE (1994) A physically based model for the topographic control on shallow landsliding. Water Resour Res 30:1153–1171

Mostbauer K, Kaitna R, Prenner D, Hrachowitz M (2018) The temporally varying roles of rainfall, snowmelt and soil moisture for debris flow initiation in a snow-dominated system. Hydrol Earth Syst Sci 22:3493–3513. https://doi.org/10.5194/hess-22-3493-2018

Nadim F, Kjekstad O, Peduzzi P, Herold C, Jaedicke C (2006) Global landslide and avalanche hotspots. Landslides 3:159–173. https://doi.org/10.1007/s10346-006-0036-1

Nambajimana J de D, He X, Zhou J et al (2020) Land use change impacts on water erosion in Rwanda. Sustain 12:1–23. https://doi.org/10.3390/SU12010050

Ngarukiyimana JP, Fu Y, Yang Y, Ogwang A (2017) Dominant atmospheric circulation patterns associated with abnormal rainfall events over Rwanda. East Africa Int J Climatol 38:187–202. https://doi.org/10.1002/joc.5169

Peres DJ, Cancelliere A, Greco R, Bogaard TA (2017) Influence of uncertain identification of triggering rainfall on the assessment of landslide early warning thresholds. Nat Hazards Earth Syst Sci Discuss:1–28. https://doi.org/10.5194/nhess-2017-328

Peruccacci S, Brunetti MT, Gariano SL, Melillo M, Rossi M, Guzzetti F (2017) Rainfall thresholds for possible landslide occurrence in Italy. Geomorphology 290:39–57. https://doi.org/10.1016/j.geomorph.2017.03.031

Petley D (2012) Global patterns of loss of life from landslides. Geology 40:927–930. https://doi.org/10.1130/G33217.1

Piller AN (2016) Precipitation intensity required for landslide initiation in Rwanda. University honors theses. Paper 274. Portland State University

Postance B, Hillier J (2017) Comparing threshold definition techniques for rainfall-induced landslides : a national assessment using radar rainfall. Earth Surf Process Landforms 560:553–560. https://doi.org/10.1002/esp.4202

Prenner D, Kaitna R, Mostbauer K, Hrachowitz M (2018) The value of using multiple Hydrometeorological variables to predict temporal debris flow susceptibility in an alpine environment. Water Resour Res 54:6822–6843. https://doi.org/10.1029/2018WR022985

Prenner D, Hrachowitz M, Kaitna R (2019) Trigger characteristics of torrential flows from high to low alpine regions in Austria. Sci Total Environ 658:958–972. https://doi.org/10.1016/j.scitotenv.2018.12.206

Robbins JC (2016) A probabilistic approach for assessing landslide-triggering event rainfall in Papua New Guinea, using TRMM satellite precipitation estimates. J Hydrol 541:296–309. https://doi.org/10.1016/j.jhydrol.2016.06.052

Roccati A, Faccini F, Luino F, Turconi L., Guzzetti F. (2018) Rainfall events with shallow landslides in the Entella catchment , Liguria , northern Italy. Nat Hazards Earth Syst Sci 18:2367–2386. https://doi.org/10.5194/nhess-18-2367-2018, Rainfall events with shallow landslides in the Entella catchment, Liguria, northern Italy

Rosso R, Rulli MC, Vannucchi G (2006) A physically based model for the hydrologic control on shallow landsliding. Water Resour Res 42:1–16. https://doi.org/10.1029/2005WR004369

van Beek R (2002) Assessment of the influence of changes in land use and climate on landslide activity in a Mediterranean environment. Universiteit Utrecht, Netherlands

J. Uwihirwe · M. Hrachowitz · T. A. Bogaard
Section Water Resources, Department of Water Management, Faculty of Civil Engineering and Geosciences,
Delft University of Technology,
PO Box 50482600 GA, Delft, The Netherlands

M. Hrachowitz
e-mail: M.Hrachowitz@tudelft.nl

T. A. Bogaard
e-mail: T.A.Bogaard@tudelft.nl

J. Uwihirwe (✉)
Department of Irrigation and Drainage, School of Agricultural Engineering, College of Agriculture Animal Sciences and Veterinary Medicine,
University of Rwanda,
PO Box 210, Musanze, Rwanda
Email: J.Uwihirwe@tudelft.nl; uwihirwejudith@yahoo.fr